Computers in Biology and Medicine 192 (2025) 110355

Contents lists available at ScienceDirect

Computers in Biology and Medicine

journal homepage: www.elsevier.com/locate/compbiomed

A new braided model of the Amulet Amplatzer for accurate simulations of left atrial appendage occlusion procedures

Rafizul Islam Md [a], Matthew T. Lee [b], Andrew C. Cook [c], Jonathan Weir-McCall [d], Claire A. Martin [e], Thomas W. Peach [b], Gaetano Burriesci [b,f,1], Giorgia M. Bosi [b,*,1]

[a] Department of Medical Physics and Biomedical Engineering, Faculty of Engineering Sciences, University College London, United Kingdom
[b] Department of Mechanical Engineering, Faculty of Engineering Sciences, University College London, United Kingdom
[c] Institute of Cardiovascular Science, Faculty of Population Health Sciences, University College London, United Kingdom
[d] Department of Radiology, University of Cambridge, United Kingdom
[e] Department of Cardiology, Royal Papworth Hospital, Cambridge, United Kingdom
[f] University of Palermo, Department of Engineering, Palermo, Italy

ARTICLE INFO

Keywords:
Patient-specific computational modelling
Left atrial appendage occlusion (LAAO)
Cardiovascular engineering
Braided model
Atrial fibrillation

ABSTRACT

Atrial Fibrillation (AF) is a cardiac disease altering the human heart rate. It is posing an increasing burden to society, with complications that lead to stroke and ischemic events from thromboembolisms, originating in the left atrial appendage (LAA). Percutaneous LAA occlusion (LAAO) is becoming an increasingly adopted preventive treatment option due to its minimally invasive nature. However, this treatment faces complex challenges: the heterogeneity of LAA morphologies limits the pre-operative planning and several procedures are associated with peri-device leakage from malposition and device-related thrombi. One of the two most commonly deployed LAAO devices (LAAODs) is the Amulet Amplatzer (AA), a mesh-like pacifier device. In-silico models have demonstrated their potential to serve as supporting tools for clinical planning, providing insight able to enhance the efficacy and safety of the intervention. Most of the computational studies approximate the AA to a closed surface model. In this work, we aimed to develop a more realistic and detailed structural model of the AA, capturing the mesh of wires. Experimental tests on the physical device were conducted to compare the behaviour of simplified closed surface models and the newly developed braided geometry. The results have demonstrated how closed surface models of the AA fail to capture the real deformation mechanism of the physical device. Conversely, the more realistic braided characterisation mimics more closely the changes in shape of the physical AA, by capturing the change in angles of the wires. Finally, the virtual deployment of the intertwined model into a patient-specific LAA resulted in a configuration similar to the clinically implanted AA.

1. Introduction

Atrial Fibrillation (AF) is a cardiac arrhythmia where the coordinated contraction of the atria is altered by irregular electrical activity of the heart [1]. It increases with age, with valve disease, and in frequency over time. The worldwide prevalence of AF has increased by 33.5 million since 2010 and, according to the Global Burden of Disease 2019 Study, 59 million people were estimated to live with AF in 2019 [2–4]. With an ageing population and improvement in diagnostic techniques, the prevalence of AF is expected to rise substantially in the next decades [5,6]. Therefore, AF has already become a 21st-century cardiovascular epidemic [7–9], and its management is a serious public health concern. Recent studies have shown that non–valvular AF is an independent risk factor that increases the reoccurrence of thromboembolic events by 4–5 folds, with over 90 % of the thrombi originating in the left atrial appendage (LAA) [10–12]. The LAA is a protruding finger-like structure and remnant of the embryonic left atrium [13]. It has greater compliance than the rest of the left atrium and, under sinus rhythm, performs active contraction to regulate left atrial pressure [14,15]. In contrast, in AF, the LAA contractility and blood flow velocity within are reduced

This article is part of a special issue entitled: Cardiovascular Digital Twins published in Computers in Biology and Medicine.

* Corresponding author.
E-mail address: g.bosi@ucl.ac.uk (G.M. Bosi).

[1] These authors contribute equally to this work and share the last authorship.

https://doi.org/10.1016/j.compbiomed.2025.110355
Received 29 November 2024; Received in revised form 29 March 2025; Accepted 5 May 2025
Available online 13 May 2025

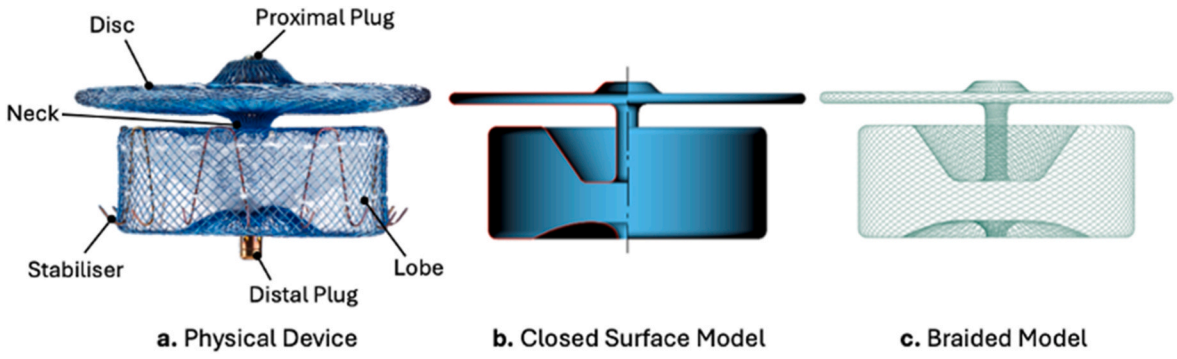

Fig. 1. (a) Illustration of the physical AA; (b) illustration of the equivalent closed surface model; (c) illustration of the braided model.

[16,17]. This altered haemodynamics condition favours blood stasis and, consequently, the formation of thrombi [18]. Therefore, mitigation of thromboembolic events is crucial as strokes due to AF lead to disability or death in 70–80 % of cases [19,20].

The most adopted preventive thromboembolic stroke treatments for the LAA are the prescription of anticoagulants, surgical LAA exclusion and percutaneous LAA occlusion (LAAO) [21]. Whilst anticoagulant therapy remains the gold standard, it presents significant disadvantages: the daily administration of medication and associated costs, and the increased risk of bleeding complications. As a result, up to 50 % of AF patients are deemed ineligible for this therapy [22–27]. Surgical LAA exclusion is highly invasive, usually performed concomitant with mitral valve surgery and with a variable success rate [28,29]. In 2018, following a systematic review of the relevant clinical studies, the National Health Service (NHS) in England published a clinical commissioning policy to support routine LAAO where the oral anticoagulant is contra-indicated [30]. LAAO is a minimally invasive procedure [31], where an occluding device is inserted via a delivery sheath or catheter usually through the femoral vein, followed by a transseptal puncture at the oval fossa to reach the LAA ostium [32]. Imaging techniques such as transoesophageal echocardiography or computed tomography are commonly adopted to inspect the LAA and take key measurements needed to select the most suitable size of the LAAO device (LAAOD) [32,33]. Then, the catheter, containing the crimped LAAOD, is advanced into the implant zone. Once the delivery system is positioned and oriented suitably, the device is deployed and adjusted until the clinician is satisfied with the device's location and anchoring; finally, the LAAOD is released from the delivery system. Due to its minimally-invasive nature, LAAO is reported to be associated with shorter operational time, shorter hospital stays and faster recovery over the surgical exclusion of the LAA [34–37].

Yet, the technique to deploy LAAODs is not trivial and, can be associated with major complications. Pre-procedural planning often involves measurements of the highly heterogeneous LAA morphology, which can be challenging when relying on two-dimensional images [38]. Post-procedural issues include peri-device leakage and late device-related thrombosis. Hence, there is room for improvement for LAAOs planning to improve adoption, treatment delivery and outcomes [39,40].

Computational modelling approaches, such as the Finite Element (FE) method, have shown significant potential as supporting tools, to aid clinicians in the selection of occluders, prediction of deployment landing and minimising peri-leaks from device malposition [41].

The most implanted LAAODs are the Watchman (Boston Scientific, Marlborough, MA, USA) and the Amulet Amplatzer (AA) (Abbott, Abbott Park, IL, USA) [42,43]. Whilst there have been more than a dozen different computational studies of the Watchman to aid pre-procedural planning [32,39,44–52], fewer *in-silico* studies are available in the literature about the AA [45–47]. Most of these focus on the haemodynamic conditions established in patient-specific LAAs after virtual LAAOD implantation, avoiding the accurate modelling of the AA structural response needed to simulate the full implantation procedure. Aguado *et al.* conduct fluid flow analysis around virtually implanted AA, modelled as a closed surface geometry, without validation of the deformed configuration in the patient-specific LAA [47]; more detailed structural features were considered by Zhong *et al.*, where only the disc of the AA was modelled by Nitinol beam elements neglecting the real mechanical structure of the rest of the device [45]. Bavo *et al.* present a structural analysis of the AA, although details on the key approaches at a modelling level of the device are not provided [46].

The urgency of well-defined computational structural LAAOD models is stressed by the recent outcomes of the Amulet IDE Trial: the largest randomised control trial to evaluate the safety and effectiveness of the two most adopted occluders. This showed that the AA is non-inferior to the Watchman in terms of primary safety end-point and that LAA occlusion was higher for the Amulet occluder than for the Watchman device. Despite procedure-related complications seemed to be higher for the AA, mainly due to operator experience, device embolisation and pericardial effusion [53–55], the AA is known to provide more flexibility in terms of deployment techniques, allowing the sandwich and the thrombi trapping methods [8,33,56]. The latter has shown the potential to expand the adoption of the AA further to include patients with LAA thrombus, who were formerly considered unsuitable for LAAO [8,56].

In this context, this work aims to provide a pipeline for the minimally-invasive virtual deployment of a model describing more realistically the implantation of the AA into the LAA, to create a supporting tool for patient-specific planning that enhances LAAO procedural efficacy and safety. While advancing on the structural limitations of the above-mentioned computational studies of the Amulet occluder, this work highlights the need for more detailed modelling of devices by comparing the status quo closed surface model with a braided one of the AA and validating the models against experimental data. Subsequently, an in-silico pipeline for the deployment of the AA into a patient-specific LAA is simulated and validated against retrospective post-operative clinical data.

2. Methods

2.1. Device model

The AA is a self-expandable LAAOD composed of 144 interwoven Nitinol wires joined at the two extremities by two end screws/plugs and thermoset to form an anchoring lobe and an occluding disc, connected through the neck (Fig. 1a). The lobe and the disc host haemostatic polyester patches. Stabilising wires are attached to the lobe to enhance anchoring. Upon deployment in the LAA, the lobe expands into the LAA preventing device migration, aided by the stabilising wires. Meanwhile, the disc covers the LAA ostium at the atrial side with the polyester patch, preventing thrombus embolisation. Since the structural behaviour of the

Table 1
Key measurements of the reconstructed AA, corresponding to the AA of size 25.

Key Variables	Mean measurements (mm)
Wire diameter, ϕ_{Wire}	0.10
Disc diameter, ϕ_{Disc}	31.70
Lobe diameter, ϕ_{Lobe}	24.78
Lobe height, h_{Lobe}	9.83

frame is essentially provided by the interlaced Nitinol wires, for this study, only the braided frame of the device is modelled. The geometry of the AA was generated in the Computer-Aided Design (CAD) software Rhinoceros (7.0, Robert McNeel, Seattle, WA, USA), based on the online AA sizing chart and measurements taken from the physical device, corresponding to the AA of size 25 [57]. An equivalent closed surface model of the device, similar to the configuration described in previous studies [46,47], was also generated, as shown in Fig. 1b. Ultimately, a more detailed model including each wire as a continuous beam structure was created (Fig. 1c). The dimensions of the main geometric parameters are noted in Table 1.

2.2. Finite element model

Both reconstructed geometries were imported in Abaqus 2019 (Dassault Systemes Simulia Corp., Providence, RI, USA). For the braided model, the interwoven wires were discretised by tied B32 beam elements with an average element size of 0.55 mm and a circular cross-section of 0.1 mm, based on physical measurements (Table 1), leading to a mesh size of 24k elements. The material used for the wires is Nitinol, a super-elastic Ni-Ti alloy whose properties depend on the exact composition, the thermomechanical processing and the working temperature [58,59]. Since in the operating condition (after expansion in the body) the material essentially works in the Hookean austenitic phase, it was modelled as isotropic linear elastic. The Young's Modulus was calibrated based on experimental tests performed on the physical device, as described below. The Poisson's ratio was set equal to 0.3, based on the literature [39]. The proximal and distal extremities of the device were connected by a set of B31 beam elements, with a Young's Modulus of two orders of magnitude greater than the B32 elements, to mimic the higher rigidity of the end screws/plugs. The braided device was simulated in Abaqus/Standard with the implicit method with a minimum time increment 1E-07 s. The intertwining was simulated by imposing tie constraints between couples of nodes, specifically positioned at the intersections between the beams defining the wires. At these ties, only the relative rotation of the connected pair of beams is allowed, while the relative linear displacements between the beams are completely restricted. This allows to approximate the real deformation mechanism, avoiding the need to model the contact among wires, as in [60], which strongly increases the computational cost of the analyses.

On the other hand, the closed surface model consisted of shell elements S4R (4-node quadrilateral, reduced integration) with an average element size of 0.16 mm and a thickness of 0.1 mm as per the wire's diameter dimension. The total mesh size was 41k elements. To achieve the same initial flexural rigidity of the real device, Young's modulus value was adjusted after the calibration of the linear elastic modulus of the braided model; the Poisson ratio was set to 0.49. Differently from the braided model, the FE solver Abaqus 2019/Dynamics Explicit (Dassault Systèmes, SIMULIA Corp., USA) was implemented for the shell model. In fact, explicit formulations are more suitable for handling the large deformation, the local instabilities, and the complex contact issues that characterise the crimping process for this model [45,46]. The ratio of kinetic to internal energy was kept below 5 % throughout the simulation, and the time increment was similar to that adopted for the implicit method.

2.3. Model calibration and validation

An in-vitro tension test was set up to calibrate the Young's Modulus of the material models in Abaqus and to validate the deformation mechanism of the two computational models. The physical AA device used to extract the model's dimensions was mounted on the ZwickiLine tensile testing machine (ZwickRoell GmbH & Co. KG, Ulm, Germany) with a 0.5 kN load cell via double-ended pin vises. Tests were performed inside a water bath set at body temperature (37 °C) to mimic the mechanical properties of the device when deployed into the patient's LAA. The lobe end was fully fixed at the bottom, whereas the disc end was connected to the moving end cross-head of the machine. The cross-head was displaced upwards by 60 mm at a speed of 1 mm/s and returned to its initial position at the same speed while ensuring that the water temperature stayed within 37 ± 1 °C for the entire duration of each test (Fig. 2a). Force-displacement data were recorded at a fixed frequency of 400 kHz [61]. To ensure the repeatability of the experiments, tests were replicated three times, and the average curve was utilised for

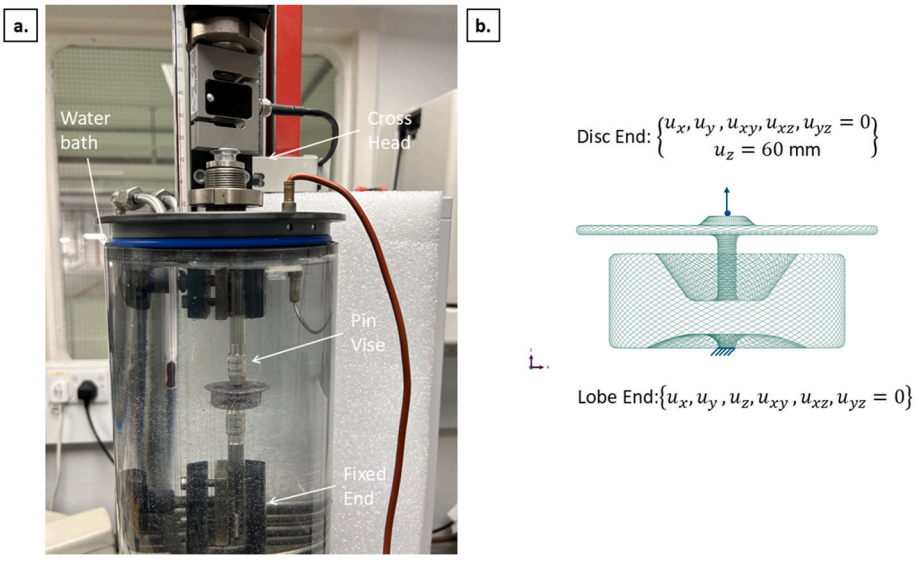

Fig. 2. a) Experimental and b) numerical set-up of the tensile test; only the braided model is represented, but the same conditions were imposed on the equivalent shell model.

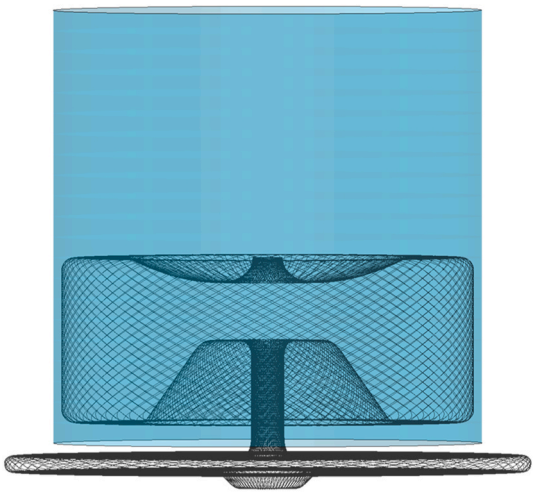

Fig. 3. Illustration of the set-up for the virtual radial test of the AA inside the concentric cylindrical surface.

comparison. To reproduce the experimental condition, the lobe end of the numerical models was fully restricted in all six degrees of freedom and the disc end was translated axially by 60 mm during loading and unloading (Fig. 2b). The linear elastic Young's Modulus of the model was adjusted accordingly to minimise the deviation from the experimental loading and unloading curves. After calibrating the Young Modulus of the computational models to achieve the same response to longitudinal loading, the radial mechanical response of the selected virtual model was determined and compared with experimental results reported in the literature [62]. An analytical cylindrical surface of a diameter larger than the lobe was positioned concentrically to the device, setting the contact only with the lobe elements (Fig. 3). Then, its diameter was gradually decreased, thus compressing the lobe of the AA in the range reported in the instructions for use [63]. The radial force was monitored for every 0.5 mm of diameter reduction.

2.4. Patient-specific anatomy reconstruction

In collaboration with the Royal Papworth Hospital NHS Foundation Trust, Cardiac Computed Tomography Angiography (CCTA) for a single AF patient was acquired before and 6 months after LAAOD implantation with an AA of size 22 (corresponding to a lobe diameter of 22 mm and a disc diameter of 28 mm). The dimensions of the images were 512 × 512 pixels, with a pixel size of 381 μm × 381 μm and a slice thickness of 750 μm, acquired with the Siemens Somatom Force (Siemens Healthcare GmbH, Erlangen, Germany). The CCTA scans were imported into the commercial post-processing software Mimics (Materialise, Materialise Inc., Leuven, Belgium) as Digital Imaging and Communications in Medicine (DICOM) (Digital Imaging and Communications in Medicine) files. The 3D geometric surface of the full left atrium was reconstructed for both scans from previously adopted manual segmentation protocols, consisting of thresholding and region-growing techniques [64–66]. Next, the implantation site was discretised into triangular elements in 3-Matic (Materialise Inc., Leuven, Belgium).

For computational efficiency, a triangulated mesh with an average elements edge length of 0.5 mm was computed for the LA and LAA, whilst the pulmonary veins and mitral valve were cut and replaced with planar open surfaces, as shown in Fig. 4 [67]. Consequently, the 3D reconstructions of the two scans were registered using the LAA ostium plane as a reference. This was necessary to infer the positioning and orientation of the AA with respect to the LAA, which is not visible in the post-operative reconstruction since the blood pool is stagnated around the AA.

2.5. Virtual deployment into patient-specific anatomy

A braided beam model of the specific AA used in the implant (i.e. size 22 mm) was generated starting from the AA 25 mm model, modifying the dimensional parameters defining the nominal dimensions to match the dimensions specified in the instruction for use manual and from the manufacturer's website for the relevant size [63]. Consequently, a numerical pipeline was developed, consisting of three steps.

1) *Positioning:* The manually registered reconstructed scans are imported into the Abaqus Assembly Module as three separate parts. Translation and rotation are applied to the three parts so that the virtual beam model of the AA sits in the landing zone of the pre-operative LAA geometry. These criteria are implemented to mimic the initial position of the AA adopted by the clinician at LAA ostium.

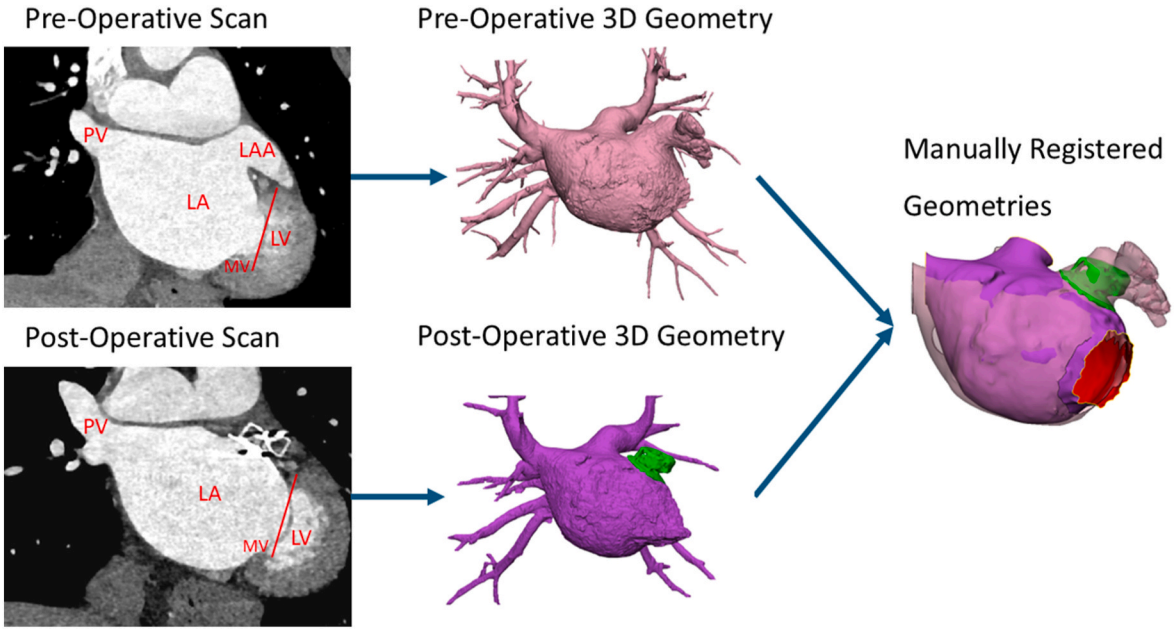

Fig. 4. Reconstruction of patient-specific pre- and post-operative scans.

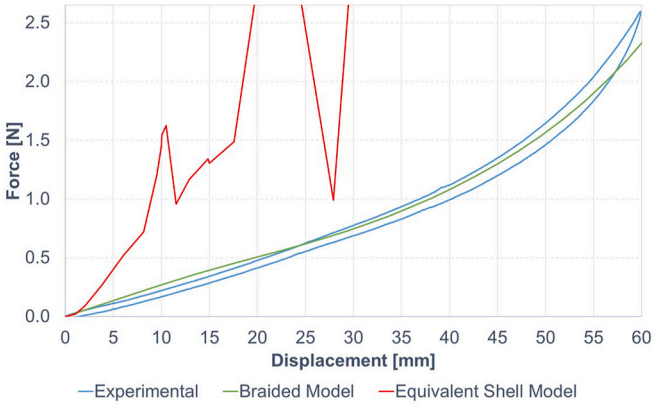

Fig. 5. Experimental and numerical tensile test curves for the calibration of the Young's Modulus of the Nitinol at 37 °C.

2) *Crimping:* The catheter sheath containing the crimped AA is modelled as a rigid hollow cylinder of 4 mm diameter and 100 mm length, with a flared funnel inlet to account for the rim of the physical sheath and to facilitate crimping. The loading is simulated by keeping the delivery tube completely stationary in all its displacement degrees of freedom whilst pulling the AA disc hub axially to fully insert the device in the tube and restricting the other displacement degrees of freedom. The patient-specific reconstructed parts from the registration are deactivated parts in this step of the simulation.
3) *Releasing:* The pre-operative LAA wall is activated at this stage and modelled by S3 elements with a thickness of 2.1 mm and with a linear elastic modulus and Poisson ratio of 1.5 MPa and 0.49, respectively [32,68]. A general contact algorithm is defined between the pre-operative LAA wall and beam elements of the AA, with hard normal contact and a friction coefficient of 0.1 [69,70]. As per the instruction for use manual of the AA [63], "Releasing" occurs in two phases: firstly, an axial displacement boundary condition at the disc end is applied until the lobe of the AA is completely pushed out of the delivery system; subsequently, the catheter is pulled back axially relatively to the device to allow the disc of the device to expand out of its crimped configuration and recoil back elastically. In both phases, a circumferential set of nodes on the LAA ostium was restricted from rotating and moving axially.

3. Results

3.1. Model calibration and validation

The force-displacement data and frame-by-frame deformation were compared for the numerical and experimental tests.

From Fig. 5, it can be noticed that the experimental curve shows some hysteresis during the loading-unloading cycle. A trade-off curve was selected at E = 102.5 GPa where the root mean squared error was 7.5 % and 8.0 % with the loading and unloading experimental curves respectively, up to 60 mm of displacement. This Young's Modulus value was utilised for the subsequent numerical simulations of the braided model. After calibrating the device's material, both numerical models were compared to the experimental tests. The flexural rigidity of the shell model was set to have the same response as the braided one at the unloaded configuration. Hence, the shell force-displacement curve started with the same slope as the braided model but deviated after the first millimetre of deformation (Fig. 5). Beyond 27 mm of displacement, the forces predicted by the shell model increased dramatically, exceeding the experimental curve by several orders of magnitude. The tensile tests for the braided and the closed surface models were run on Intel Xeon Gold 6248 with 2.5 GHz processors using 16 cores and 16 GB of RAM, and required 28 min and 52 h, respectively.

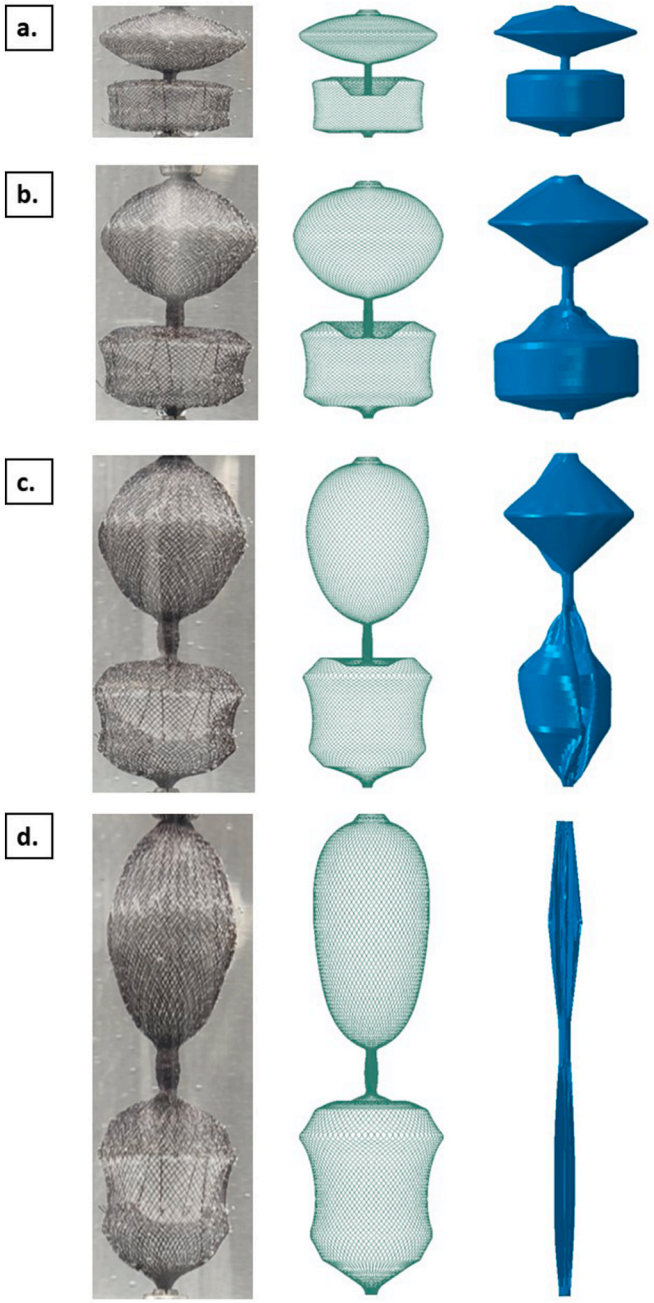

Fig. 6. Deformation mechanism of the physical AA, braided and shell models at a) 15 mm displacement; b) 30 mm displacement; c) 45 mm displacement; d) 60 mm displacement.

Key deformation frames reveal that the shell model experiences significant distortions during loading compared to the corresponding physical model. The applied displacement produces local instabilities resulting in folds on the disc during the initial stages (Fig. 6a). Then, a reversal of curvature in surfaces connecting the lobe cylindrical surface to the hub and neck (Fig. 6b) is observed, followed by folds forming in the lobe (Fig. 6c). Ultimately, a heavily creased, crimped configuration is reached between 55 and 60 mm of displacement, when the physical device still shows a semi-expanded configuration (Fig. 6d). Conversely, the braided model more accurately replicates the shape changes observed in the physical AA during loading (Fig. 6a–d).

Moreover, while the braided model returns to its original configuration when released, in the case of the shell model, the local instabilities experienced during crimping lead to unloaded equilibrium

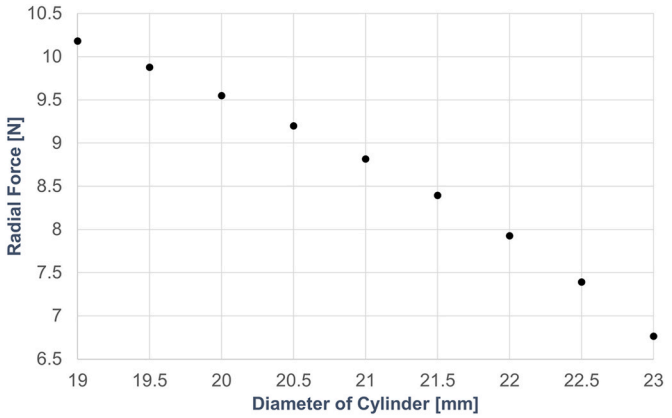

Fig. 7. Illustration of the radial stiffness of the virtual braided model.

configurations that are characterised by the presence of residual stresses and are different from the original.

Hence, the shell model resulted unsuitable to simulate the virtual patient-specific implantation, which was performed with the braided model only.

After selecting the braided computational model, its mechanical response was validated in the radial direction. Simulations indicate an increase in the measured radial force by 1 N for every 1 mm reduction in the landing zone diameter (Fig. 7). This well replicates the behaviour obtained by Menne *et al.* from experimental radial loading tests performed on a segmented head apparatus, at 37 °C [62]. This response was independent of the size of the AA.

3.2. Virtual deployment into patient-specific anatomy

Fig. 8 depicts the release of the AA in the patient-specific LAA from its crimped configuration (Fig. 8a). The interaction with the LAA causes the lobe of the AA to deform at an angle with respect to its disc, affected by the LAA's morphology, rigidity and thickness (Fig. 8b and c). During the retraction of the catheter, the disc recoils back elastically and covers successfully the LAA ostium, as per its intended use (Fig. 9). A relative angle between the lobe and the neck of the device and the thickening of the disc when in contact with the LAA wall are obtained, which well replicate the AA implanted in the patient's LAA (see Fig. 9).

The maximum strain was observed to be 0.5 % in its operating condition (i.e. the expanded configuration in the patient's anatomy), which is well below the typical phase transformation strain (from austenite to martensite) of the material, which for this type of applications is commonly reported in the range of 1 % [71]. This confirms the validity of a linear elastic model for the analysis of the working condition.

The numerical pipeline was completed in about 62 h with Intel Xeon Gold 6248 2.5 GHz processors using 16 cores and 16 GB of RAM.

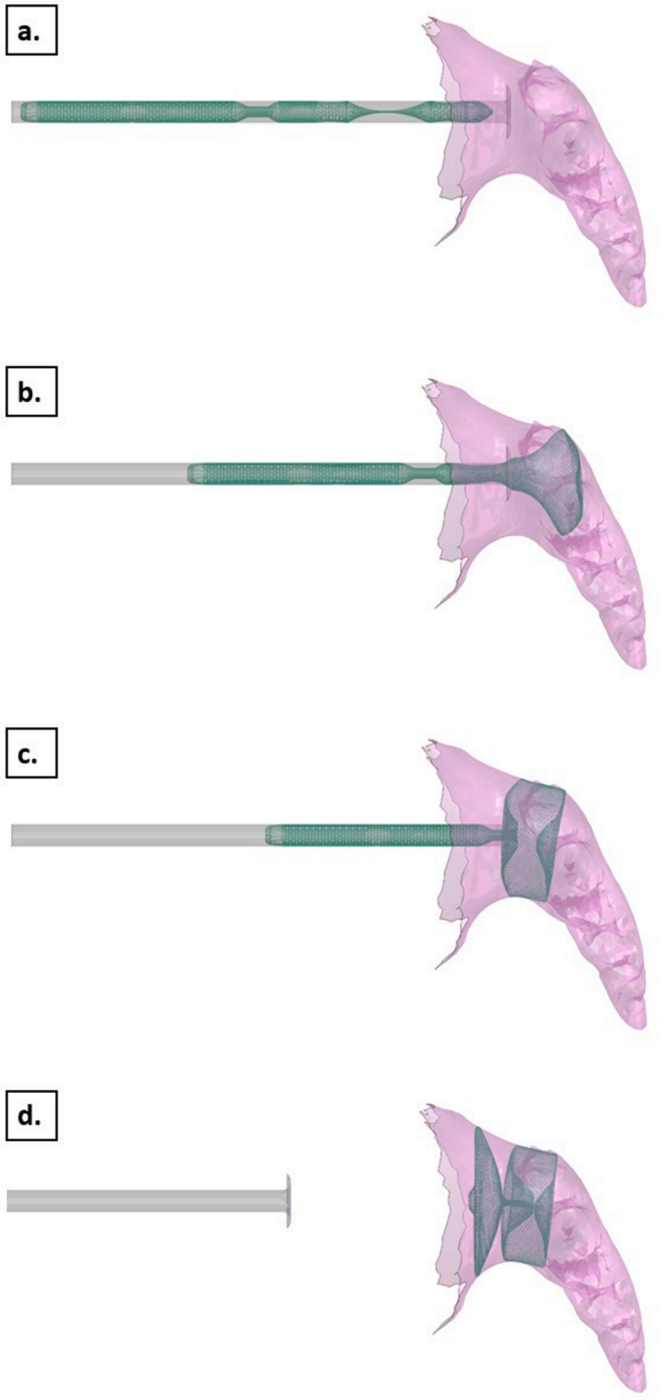

Fig. 8. Deployment of the AA in the LAA a) crimped AA; b) AA interaction with LAA; c) lobe expansion; d) disc apposition.

4. Discussion

In this work, the model of the mesh-like AA has been created and compared with experimental tests on a physical device and with a state-of-the-art closed surface virtual model; then, it was deployed in a virtual patient-specific LAA to mimic the minimally invasive procedure, aiming to create a digital twin supporting tool for tailored therapy planning and to enhance the treatment's safety and efficacy.

Starting from measurements of the AA, a braided geometry was reconstructed alongside an equivalent surface closed model, representing the most common approach adopted in past studies [45,47]. In-vitro tests were carried out for calibration of the device's material, performed at the operating temperature of the AA inside the LAA. Larger deviations from the experimental data are noted at high displacement values, which would require a more detailed material model definition than a linear elastic one, able to describe the stress-induced phase transformation associated with the super-elastic behaviour. Nevertheless, given that for the typical post-implant operating conditions of the AA are associated with strain levels below the upper transformation plateau (a maximum oversizing of 30 % is recommended by the manufacturer) [71], the linear elastic material model was deemed reasonable.

During the validation of the model, it was shown that, despite having the same initial flexural rigidity (Fig. 5), the shell model quickly becomes far more rigid exhibiting higher forces for the same displacement compared to the braided model. To undergo large deformations, the

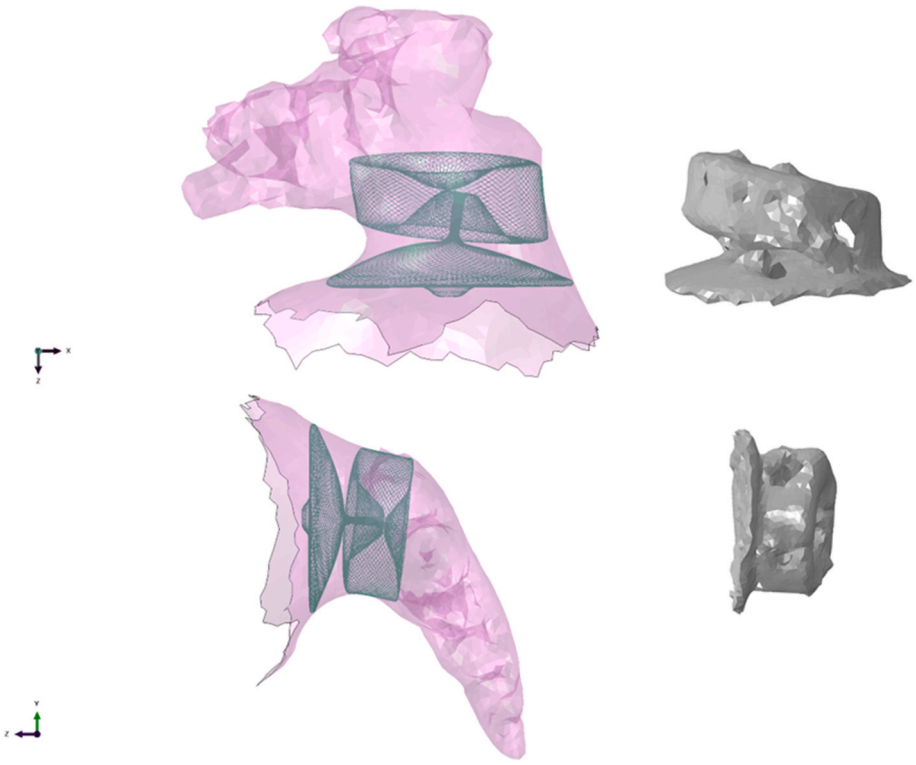

Fig. 9. Side-by-side deformed configuration of the virtual beam model (on the left) and reconstructed post-operative AA obtained clinical images (on the right), as shown in Fig. 3, from two different orthogonal points of view.

closed surface model demonstrates local numerical instabilities in terms of buckling that led to folding, such as at the disc (Fig. 6a) and the lobe (Fig. 6c) as well as snap-through mechanisms at the regions joining the lobe's cylindrical surface with the distal hub and with the neck. These snap-through events cause the initially concave neck-lobe and lobe-hub regions to transition into stable convex states, which do not return to the initial unstressed configuration upon removal of the load (Fig. 6b). This would make the simulation of the device release inaccurate. Ultimately, the shell model stabilises in a creased configuration (Fig. 6d). The formation of folds and the snap-through of the lobe-hub and neck-lobe regions are anticipated by large increases of rigidity, followed by sudden reductions when the associated local buckling and curvature reversals have occurred. Hence, the force-displacement diagram obtained for the shell model is characterised by large oscillations.

On the other hand, the virtual braided model appears to better replicate the experimental behaviour, following a continuous J-shape curve (Fig. 5). By capturing the changes in angles of the interwoven wires, the braided model presents an overall low rigidity of the structure in the first 30 mm of displacement (Figs. 5, 6a and b). This phase corresponds to the expansion of the disc into a more ballon-like shape, mirroring the behaviour of the physical model. The structure becomes progressively more rigid beyond 30 mm of displacement, due to the increased density of the wires in the disc and in the lobe; these regions experience radial compression as the axial stretching increases (Fig. 6c and d), closely matching the behaviour of the experimental AA. By modelling the change in angles and density of wires, the virtual braided model successfully captures the local rigidity and Poisson's ratio across different zones and stages of deformation.

Moreover, given the computational time discrepancies, the quantitative (Fig. 5) and qualitative comparisons (Fig. 6) of the two virtual models with respect to the physical device, we believe that the implicit braided model has the potential to provide more valuable insights than the explicit closed surface model.

This process confirms that the design choice adopted in the AA to use of a nitinol mesh confers to the device a unique operating mechanics and a geometrical stability during loading and release which is difficult to achieve with other strategies.

As a proof of concept, the beam model was then deployed virtually into a single patient-specific pre-operative LAA. Since the position and orientation of the delivery system of the procedure were not known, some difference between the clinical reconstructed AA and numerical configurations was expected. Still, the simulation successfully captured the main implantation mechanisms and resulted in similar features in the post-procedural configuration. The virtual deployment of the model has successfully simulated the implantation procedure, achieving a final configuration covering entirely the LAA ostium, thanks to a pulling action produced by the tension determined in the neck. Similarly to the implanted physical device, the model lobe has taken a swayed shape, interacting with the LAA wall morphology. This suggests that the proposed approach can effectively provide useful predictive clinical indications, anticipating the behaviour of the final configuration of the device and potentially minimising the risk of peri-device leakage.

However, the application on a single clinical procedure still demands for further validation [72–75], extended to a larger patient database. Moreover, the CCTA scans were not ECG gated, and the pre- and post-operative scans are likely to be in different cardiac phases (Fig. 4). Furthermore, with the blood pool's absence inside the post-operative LAA morphology due to the implanted AA, it is impossible to quantify the extent of LAA remodelling and whether this has impacted the implant configuration over time [76]. For the same reasons, a quantitative comparison of the effectiveness of LAA occlusion with the post-operative scan in terms of peri-device leakage could not be performed in this study as the post-operative LAA is not visible from the CCTA reconstruction.

5. Conclusion

LAAO is becoming increasingly adopted to prevent thromboembolic

events in AF patients. Nevertheless, the deployment of these LAAODs can be associated with post-procedural peri-device leak and complications, which can be minimised by specific operator pre-implant training and procedural planning. Computational modelling represents a tool that can support clinicians in making more insightful decisions to enhance patients' treatment outcomes. The developed pipeline advances the current modelling framework for LAAOD and AA in particular; the virtual braided model appears to be able to replicate the deformation mechanism observed experimentally and reproduce the AA's configuration in patient-specific LAA settings. The developed computational framework, once validated on a larger number of cases, could represent a valid tool to anticipate, and thereby minimise potential complications, and support device selection and procedural planning.

CRediT authorship contribution statement

Rafizul Islam Md: Writing – original draft, Visualization, Software, Methodology, Formal analysis, Data curation, Conceptualization. **Matthew T. Lee:** Software, Methodology, Formal analysis, Data curation. **Andrew C. Cook:** Writing – review & editing, Data curation. **Jonathan Weir-McCall:** Data curation. **Claire A. Martin:** Data curation. **Thomas W. Peach:** Methodology, Data curation. **Gaetano Burriesci:** Writing – review & editing, Supervision, Methodology, Formal analysis, Conceptualization. **Giorgia M. Bosi:** Writing – review & editing, Supervision, Methodology, Formal analysis, Conceptualization.

Ethical information

The project was reviewed by the Royal Papworth Hospital governance team and granted permission with project reference S02806.

Funding

This work was supported by funding from the Engineering, and Physical Sciences Research Council (EPSRC), the UCL Centre for Doctoral Training in Intelligence, and Integrated Imaging in Healthcare (i4health) [EP/S021930/1]; the Royal Academy of Engineering Fellowship (RF/201920/19/221); the British Heart Foundation (FS/4yPhD/F/20/34134), The Wellcome (310796/Z/24/Z) & Additional Ventures (Award: 1019894).

Declaration of competing interest

Andrew C. Cook is a speaker and consultant for Abbott, Atricure, Occlutech, Edwards, Heartworks and Babyworks and an advisory board member for Abbott Cardiovascular.

Acknowledgements

The authors greatly acknowledge the support from the Royal Papworth Hospital NHS Foundation Trust.

Appendix A. Supplementary data

Supplementary data to this article can be found online at https://doi.org/10.1016/j.compbiomed.2025.110355.

References

[1] Z. Nesheiwat, A. Goyal, M. Jagtap, Atrial fibrillation, in: StatPearls, StatPearls Publishing, Treasure Island (FL), 2023. http://www.ncbi.nlm.nih.gov/books/NBK526072/. (Accessed 13 August 2023).

[2] G.A. Roth, G.A. Mensah, C.O. Johnson, G. Addolorato, E. Ammirati, L.M. Baddour, N.C. Barengo, A.Z. Beaton, E.J. Benjamin, C.P. Benziger, A. Bonny, M. Brauer, M. Brodmann, T.J. Cahill, J. Carapetis, A.L. Catapano, S.S. Chugh, L.T. Cooper, J. Coresh, M. Criqui, N. DeCleene, K.A. Eagle, S. Emmons-Bell, V.L. Feigin, J. Fernández-Solà, G. Fowkes, E. Gakidou, S.M. Grundy, F.J. He, G. Howard, F. Hu, L. Inker, G. Karthikeyan, N. Kassebaum, W. Koroshetz, C. Lavie, D. Lloyd-Jones, H. S. Lu, A. Mirijello, A.M. Temesgen, A. Mokdad, A.E. Moran, P. Muntner, J. Narula, B. Neal, M. Ntsekhe, G. Moraes de Oliveira, C. Otto, M. Owolabi, M. Pratt, S. Rajagopalan, M. Reitsma, A.L.P. Ribeiro, N. Rigotti, A. Rodgers, C. Sable, S. Shakil, K. Sliwa-Hahnle, B. Stark, J. Sundström, P. Timpel, I.M. Tleyjeh, M. Valgimigli, T. Vos, P.K. Whelton, M. Yacoub, L. Zuhlke, C. Murray, V. Fuster, GBD-NHLBI-JACC global burden of cardiovascular diseases writing group, global burden of cardiovascular diseases and risk factors, 1990-2019: update from the GBD 2019 study, J. Am. Coll. Cardiol. 76 (2020) 2982–3021, https://doi.org/10.1016/j.jacc.2020.11.010.

[3] S.S. Chugh, R. Havmoeller, K. Narayanan, D. Singh, M. Rienstra, E.J. Benjamin, R. F. Gillum, Y.-H. Kim, J.H. McAnulty, Z.-J. Zheng, M.H. Forouzanfar, M. Naghavi, G. A. Mensah, M. Ezzati, C.J.L. Murray, Worldwide epidemiology of atrial fibrillation: a global burden of disease 2010 study, Circulation 129 (2014) 837–847, https://doi.org/10.1161/CIRCULATIONAHA.113.005119.

[4] D. Linz, M. Gawalko, K. Betz, J.M. Hendriks, G.Y.H. Lip, N. Vinter, Y. Guo, S. Johnsen, Atrial fibrillation: epidemiology, screening and digital health, Lancet Reg. Health - Eur. 37 (2024) 100786, https://doi.org/10.1016/j.lanepe.2023.100786.

[5] M. Zoni-Berisso, F. Lercari, T. Carazza, S. Domenicucci, Epidemiology of atrial fibrillation: European perspective, Clin. Epidemiol. (2014) 213, https://doi.org/10.2147/CLEP.S47385.

[6] L. Bencivenga, K. Komici, P. Nocella, F.V. Grieco, A. Spezzano, B. Puzone, A. Cannavo, A. Cittadini, G. Corbi, N. Ferrara, G. Rengo, Atrial fibrillation in the elderly: a risk factor beyond stroke, Ageing Res. Rev. 61 (2020) 101092, https://doi.org/10.1016/j.arr.2020.101092.

[7] J. Kornej, C.S. Börschel, E.J. Benjamin, R.B. Schnabel, Epidemiology of atrial fibrillation in the 21st century: novel methods and new insights, Circ. Res. 127 (2020) 4–20, https://doi.org/10.1161/CIRCRESAHA.120.316340.

[8] Z. Zhang, J. Zhou, Q. Lin, C. Wang, Y. Huang, Y. Dai, W. Zuo, N. Liu, Y. Xiao, Q. Liu, Overcoming barriers for left atrial appendage thrombus: a systematic review of left atrial appendage closure, BMC Cardiovasc. Disord. 24 (2024) 175, https://doi.org/10.1186/s12872-024-03843-w.

[9] C.T. January, L.S. Wann, H. Calkins, L.Y. Chen, J.E. Cigarroa, J.C. Cleveland, P. T. Ellinor, M.D. Ezekowitz, M.E. Field, K.L. Furie, P.A. Heidenreich, K.T. Murray, J. B. Shea, C.M. Tracy, C.W. Yancy, AHA/ACC/HRS focused update of the 2014 AHA/ACC/HRS guideline for the management of patients with atrial fibrillation: a report of the American College of cardiology/American heart association task force on clinical practice guidelines and the heart rhythm society in collaboration with the society of thoracic surgeons, Circulation 140 (2019) e125–e151, https://doi.org/10.1161/CIR.0000000000000665, 2019.

[10] C. Marini, F. De Santis, S. Sacco, T. Russo, L. Olivieri, R. Totaro, A. Carolei, Contribution of atrial fibrillation to incidence and outcome of ischemic stroke, Stroke 36 (2005) 1115–1119, https://doi.org/10.1161/01.STR.0000166053.83476.4a.

[11] G.Y.H. Lip, B. Freedman, R.D. Caterina, T.S. Potpara, Stroke prevention in atrial fibrillation: past, present and future, Thromb. Haemost. 117 (2017) 1230–1239, https://doi.org/10.1160/TH16-11-0876.

[12] D. Linz, A. Hermans, R.G. Tieleman, Early atrial fibrillation detection and the transition to comprehensive management, EPP Eur. 23 (2021) ii46–ii51, https://doi.org/10.1093/europace/euaa424.

[13] S. Yaghi, C. Song, W.A. Gray, K.L. Furie, M.S.V. Elkind, H. Kamel, Left atrial appendage function and stroke risk, Stroke 46 (2015) 3554–3559, https://doi.org/10.1161/STROKEAHA.115.011273.

[14] T. Mendes Silva, G. Brandão De Oliveira, T. Lins De Souza Barros, A. Barbosa De Andrade, B. Bom Furlan, M.D.C. De Pereira Nunes, Left atrial appendage: anatomy, function, and importance in thrombus formation, ABC Imagem Cardiovasc 35 (2022), https://doi.org/10.47593/2675-312X/20223502eabc301. Graduate Program in Sciences Applied to Adult Health, School of Medicine, Federal University of Minas Gerais, Belo Horizonte, MG, Brazil.

[15] N.M. Al-Saady, O.A. Obel, A.J. Camm, Left atrial appendage: structure, function, and role in thromboembolism, Heart 82 (1999) 547–554, https://doi.org/10.1136/hrt.82.5.547.

[16] C. Pollick, D. Taylor, Assessment of left atrial appendage function by transesophageal echocardiography: implications for the development of thrombus, Circulation 84 (1991) 223–231, https://doi.org/10.1161/01.CIR.84.1.223.

[17] G. Nucifora, F.F. Faletra, F. Regoli, E. Pasotti, G. Pedrazzini, T. Moccetti, A. Auricchio, Evaluation of the left atrial appendage with real-time 3-dimensional transesophageal echocardiography implications for catheter-based left atrial appendage closure, Circ, Cardiovasc. Imaging 4 (2011) 514–523, https://doi.org/10.1161/CIRCIMAGING.111.963892.

[18] A. Kushner, W.P. West, M.Z. Khan Suheb, L.S. Pillarisetty, Virchow triad, in: StatPearls, StatPearls Publishing, Treasure Island (FL), 2023. http://www.ncbi.nlm.nih.gov/books/NBK539697/. (Accessed 14 August 2023).

[19] D.J. Gladstone, E. Bui, J. Fang, A. Laupacis, M.P. Lindsay, J.V. Tu, F.L. Silver, M. K. Kapral, Potentially preventable strokes in high-risk patients with atrial fibrillation who are not adequately anticoagulated, Stroke 40 (2009) 235–240, https://doi.org/10.1161/STROKEAHA.108.516344.

[20] G. Saposnik, D. Gladstone, R. Raptis, L. Zhou, R.G. Hart, Investigators of the registry of the Canadian stroke network (RCSN) and the stroke outcomes Research Canada (SORCan) working group, atrial fibrillation in ischemic stroke: predicting response to thrombolysis and clinical outcomes, Stroke 44 (2013) 99–104, https://doi.org/10.1161/STROKEAHA.112.676551.

[21] U. Landmesser, C. Skurk, A. Tzikas, V. Falk, V.Y. Reddy, S. Windecker, Left atrial appendage closure for stroke prevention in atrial fibrillation: current status and perspectives, Eur. Heart J. (2024), https://doi.org/10.1093/eurheartj/ehae398 ehae398.

[22] E. Birman-Deych, M.J. Radford, D.S. Nilasena, B.F. Gage, Use and effectiveness of warfarin in medicare beneficiaries with atrial fibrillation, Stroke 37 (2006) 1070–1074, https://doi.org/10.1161/01.STR.0000208294.46968.a4.

[23] L.M. Brass, H.M. Krumholz, J.M. Scinto, M. Radford, Warfarin use among patients with atrial fibrillation, Stroke 28 (1997) 2382–2389, https://doi.org/10.1161/01.STR.28.12.2382.

[24] H. Zhai, L. Kang, Y. Li, X. Zhao, Q. Chu, R. Li, The progress of percutaneous left atrial appendage occlusion: a bibliometric analysis from 1994 to 2022, Medicine (Baltim.) 103 (2024) e37742, https://doi.org/10.1097/MD.0000000000037742.

[25] A.M. Alshehri, Stroke in atrial fibrillation: review of risk stratification and preventive therapy, J. Fam. Community Med. 26 (2019) 92–97, https://doi.org/10.4103/jfcm.JFCM_99_18.

[26] I. del Conde, J.L. Halperin, Ineligibility for anticoagulation in patients with atrial fibrillation, Am. J. Med. 126 (2013) 105–111, https://doi.org/10.1016/j.amjmed.2012.07.001.

[27] R. Shameem, J. Ansell, Disadvantages of VKA and requirements for novel anticoagulants, Best Pract. Res. Clin. Haematol. 26 (2013) 103–114, https://doi.org/10.1016/j.beha.2013.07.009.

[28] J. Garg, R. Kabra, R. Gopinathannair, L. Di Biase, D.D. Wang, J. Saw, R. Hahn, J. V. Freeman, C.R. Ellis, D. Lakkireddy, State of the art in left atrial appendage occlusion, JACC Clin. Electrophysiol. 11 (2025) 602–641, https://doi.org/10.1016/j.jacep.2024.10.024.

[29] K. Bartus, F.T. Han, J. Bednarek, J. Myc, B. Kapelak, J. Sadowski, J. Lelakowski, S. Bartus, S.J. Yakubov, R.J. Lee, Percutaneous left atrial appendage suture ligation using the LARIAT device in patients with atrial fibrillation, J. Am. Coll. Cardiol. 62 (2013) 108–118, https://doi.org/10.1016/j.jacc.2012.06.046.

[30] NHS England » Clinical Commissioning Policy: Left Atrial Appendage Occlusion for patients with atrial fibrillation and relative or absolute contraindications to anticoagulation (adults), (n.d.). https://www.england.nhs.uk/publication/clinical-commissioning-policy-left-atrial-appendage-occlusion-for-patients-with-atrial-fibrillation-and-relative-or-absolute-contraindications-to-anticoagulation-adults/ (accessed August 15, 2023).

[31] WATCHMAN Device (Left Atrial Appendage Closure), LOGAN WEIHE (n.d.). https://www.loganweihevisuals.com/watchman-device-left-atrial-appendage-closure (accessed September 16, 2024).

[32] F. Danielli, F. Berti, B.M. Fanni, E. Gasparotti, S. Celi, G. Pennati, L. Petrini, Left atrial appendage occlusion: On the need of a numerical model to simulate the implant procedure, Int. J. Numer. Methods Biomed. Eng. n/a (n.d.) e3814. https://doi.org/10.1002/cnm.3814.

[33] A. Tzikas, S. Gafoor, D. Meerkin, X. Freixa, I. Cruz-González, T. Lewalter, J. Saw, S. Berti, J. Nielsen-Kudsk, R. Ibrahim, D. Lakkireddy, V. Paul, D. Arzamendi, F. Nietlispach, S. Worthley, D. Hildick-Smith, J.-B. Thambo, C. Tondo, A. Aminian, Z. Kalarus, B. Schmidt, L. Søndergaard, J. Kefer, B. Meier, J.-W. Park, H. Sievert, H. Omran, Left atrial appendage occlusion with the AMPLATZER Amulet device: an expert consensus step-by-step approach, (n.d.). https://doi.org/10.4244/EIJV11I13A292.

[34] F. Labori, J. Persson, C. Bonander, K. Jood, M. Svensson, Cost-effectiveness analysis of left atrial appendage occlusion in patients with atrial fibrillation and contraindication to oral anticoagulation, Eur. Heart J. 43 (2022) 1348–1356, https://doi.org/10.1093/eurheartj/ehab847.

[35] S.M. Singh, F. Qui, H.C. Wijeysundera, Long-term clinical outcomes in contemporary patients undergoing left atrial appendage occlusion procedures in ontario, Canada, CJC Open 5 (2023) 770–778, https://doi.org/10.1016/j.cjco.2023.07.006.

[36] G.X. Wong, G.D. Singh, Transcatheter Left Atrial Appendage Closure, Methodist DeBakey Cardiovasc. J. 19 (n.d.) 67–77. https://doi.org/10.14797/mdcvj.1215.

[37] L.A.P. Dallan, H.G. Bezerra, A. Cochet, A. Kobayashi, G.F. Attizzani, I. Rashid, S. Rajagopalan, D.I. Simon, M.H. Shishehbor, M. Arruda, S.J. Filby, Safety, efficacy, and cost-effectiveness of same-day discharge for left atrial appendage occlusion, J. Invasive Cardiol. 34 (2022) E124–E131, https://doi.org/10.25270/jic/21.00142.

[38] W.D. Kim, I. Cho, Y.D. Kim, M.J. Cha, S.-W. Kim, Y. Choi, S.Y. Shin, Improving left atrial appendage occlusion device size determination by three-dimensional printing-based preprocedural simulation, Front. Cardiovasc. Med. 9 (2022), https://doi.org/10.3389/fcvm.2022.830062.

[39] A. Zaccaria, F. Danielli, E. Gasparotti, B.M. Fanni, S. Celi, G. Pennati, L. Petrini, Left atrial appendage occlusion device: development and validation of a finite element model, Med. Eng. Phys. 82 (2020) 104–118, https://doi.org/10.1016/j.medengphy.2020.05.019.

[40] M.K. Turagam, P. Velagapudi, S. Kar, D. Holmes, V.Y. Reddy, M.M. Refaat, L. Di Biase, A. Al-Ahmed, M.K. Chung, T. Lewalter, J. Edgerton, J. Cox, J. Fisher, A. Natale, D.R. Lakkireddy, Cardiovascular therapies targeting left atrial appendage, J. Am. Coll. Cardiol. 72 (2018) 448–463, https://doi.org/10.1016/j.jacc.2018.05.048.

[41] O. De Backer, X. Iriart, J. Kefer, J.E. Nielsen-Kudsk, A. Aminian, L. Rosseel, K. F. Kofoed, J. Odenstedt, S. Berti, J. Saw, L. Søndergaard, P. Garot, Impact of computational modeling on transcatheter left atrial appendage closure efficiency and outcomes, JACC Cardiovasc. Interv. 16 (2023) 655–666, https://doi.org/10.1016/j.jcin.2023.01.008.

[42] J. Qiao, B. Zhang, J. Wang, L. Pan, T. Cheng, Y. Wang, E. Xiong, Comparison between amplatzer and watchman left atrial appendage closure devices for stroke prevention in atrial fibrillation: a systematic review and meta-analysis, Cardiology 147 (2022) 290–297, https://doi.org/10.1159/000524626.

[43] V. Jaiswal, S.P. Ang, A.B. Shrestha, Z. Wajid, E.O. Endurance, F.S. Ayoobkhan, S. Khan, V. Garimellla, H. Huang, M. Ghanim, D. Song, P. Sharma, M.C. Alraies, M. Biswas, Amplatzer amulet versus watchman device for percutaneous left atrial appendage closure: a systematic review and meta-analysis, Medicine (Baltim.) 102 (2023) e34185, https://doi.org/10.1097/MD.0000000000034185.

[44] L.S. Ranard, T.P. Vahl, R. Sommer, V. Ng, J. Leb, K. Lehenbauer, P. Sitticharoenchai, O. Khalique, N. Hamid, B.M. De, A. Bavo, R.T. Hahn, FEops HEARTguide patient-specific computational simulations for WATCHMAN FLX left atrial appendage closure, JACC Adv 1 (2022) 100139, https://doi.org/10.1016/j.jacadv.2022.100139.

[45] Z. Zhong, Y. Gao, S. Kovács, V. Vij, D. Nelles, L. Spano, G. Nickenig, S. Sonntag, O. De Backer, L. Søndergaard, A. Sedaghat, P. Mela, Impact of left atrial appendage occlusion device position on potential determinants of device-related thrombus: a patient-specific in silico study, Clin. Res. Cardiol. (2023), https://doi.org/10.1007/s00392-023-02228-x.

[46] A.M. Bavo, B.T. Wilkins, P. Garot, S. De Bock, J. Saw, L. Søndergaard, O. De Backer, F. Iannaccone, Validation of a computational model aiming to optimize preprocedural planning in percutaneous left atrial appendage closure, J. Cardiovasc. Comput. Tomogr. 14 (2020) 149–154, https://doi.org/10.1016/j.jcct.2019.08.010.

[47] A.M. Aguado, A.L. Olivares, C. Yagüe, E. Silva, M. Nuñez-García, Á. Fernandez-Quilez, J. Mill, I. Genua, D. Arzamendi, T. De Potter, X. Freixa, O. Camara, In silico optimization of left atrial appendage occluder implantation using interactive and modeling tools, Front. Physiol. 10 (2019) 237, https://doi.org/10.3389/fphys.2019.00237.

[48] E. Planas, J. Mill, A.L. Olivares, X. Morales, M.I. Pons, X. Iriart, H. Cochet, O. Camara, In-silico analysis of device-related thrombosis for different left atrial appendage occluder settings, in: E. Puyol Antón, M. Pop, C. Martín-Isla, M. Sermesant, A. Suinesiaputra, O. Camara, K. Lekadir, A. Young (Eds.), Stat. Atlases Comput. Models Heart Multi-Dis. Multi-View Multi-Cent. Right Ventricular Segmentation Card. MRI Chall., Springer International Publishing, Cham, 2022, pp. 160–168, https://doi.org/10.1007/978-3-030-93722-5_18.

[49] P. Garot, X. Iriart, A. Aminian, J. Kefer, X. Freixa, I. Cruz-Gonzalez, S. Berti, L. Rosseel, R. Ibrahim, K. Korsholm, J. Odenstedt, J.-E. Nielsen-Kudsk, J. Saw, L. Sondergaard, O. De Backer, Value of FEops HEARTguide patient-specific computational simulations in the planning of left atrial appendage closure with the Amplatzer Amulet closure device: rationale and design of the PREDICT-LAA study, Open Heart 7 (2020) e001326, https://doi.org/10.1136/openhrt-2020-001326.

[50] C. Albors, A.L. Olivares, X. Iriart, H. Cochet, J. Mill, O. Camara, Impact of blood rheological strategies on the optimization of patient-specific LAAO configurations for thrombus assessment, in: O. Bernard, P. Clarysse, N. Duchateau, J. Ohayon, M. Viallon (Eds.), Funct. Imaging Model. Heart, Springer Nature Switzerland, Cham, 2023, pp. 485–494, https://doi.org/10.1007/978-3-031-35302-4_50.

[51] C. Albors, J. Mill, A.L. Olivares, X. Iriart, H. Cochet, O. Camara, Impact of occluder device configurations, in: Silico Left Atrial Hemodynamics for the Analysis of Device-Related Thrombus, 2024, https://doi.org/10.1101/2024.01.11.575154, 2024.01.11.575154.

[52] B.J. Vogl, E. Vitale, S. Ahn, A. Sularz, A. Chavez Ponce, G.V. Lo Russo, J. Collins, A. M. Bavo, A. El Shaer, A. Kramer, Y. Jia, D. Lulic, M. De Beule, J.E. Nielsen-Kudsk, O. De Backer, M. Alkhouli, H. Hatoum, Flow dynamic factors correlated with device-related thrombosis after left atrial appendage occlusion, JACC Adv 3 (2024) 101339, https://doi.org/10.1016/j.jacadv.2024.101339.

[53] D. Lakkireddy, D. Thaler, C.R. Ellis, V. Swarup, L. Sondergaard, J. Carroll, M. R. Gold, J. Hermiller, H.-C. Diener, B. Schmidt, L. MacDonald, M. Mansour, B. Maini, L. O'Brien, S. Windecker, null null, Amplatzer amulet left atrial appendage occluder versus watchman device for stroke prophylaxis (amulet IDE): a randomized, controlled trial, Circulation 144 (2021) 1543–1552, https://doi.org/10.1161/CIRCULATIONAHA.121.057063.

[54] D. Lakkireddy, J.E. Nielsen-Kudsk, S. Windecker, D. Thaler, M.J. Price, A. Gambhir, N. Gupta, K. Koulogiannis, L. Marcoff, A. Mediratta, J.A. Anderson, R. Gage, C. R. Ellis, Mechanisms, predictors, and evolution of severe peri-device leaks with two different left atrial appendage occluders, EPP Eur. 25 (2023) euad237, https://doi.org/10.1093/europace/euad237.

[55] K. Korsholm, A. Kramer, A. Andersen, J. Saw, B.L. Nørgaard, J.M. Jensen, J. E. Nielsen-Kudsk, Left atrial appendage sealing performance of the Amplatzer Amulet and Watchman FLX device, J. Intervent. Card Electrophysiol. 66 (2023) 391–401, https://doi.org/10.1007/s10840-022-01336-4.

[56] Z. Jalal, X. Iriart, M.-L. Dinet, J.-B. Selly, N. Tafer, P. Renou, I. Sibon, J.-B. Thambo, Extending percutaneous left atrial appendage closure indications using the AMPLATZER™ Cardiac Plug device in patients with persistent left atrial appendage thrombus: the thrombus trapping technique, Arch. Cardiovasc. Dis. 109 (2016) 659–666, https://doi.org/10.1016/j.acvd.2016.02.012.

[57] Amplatzer Amulet LAA Occluder | Abbott, (n.d.). https://www.cardiovascular.abbott/us/en/hcp/products/structural-heart/structural-interventions/amplatzer-amulet.html (accessed November 23, 2024).

[58] M.J. Alshannag, A.S. Alqarni, M.M. Higazey, Superelastic nickel–titanium (NiTi)-Based smart alloys for enhancing the performance of concrete structures, Materials 16 (2023) 4333, https://doi.org/10.3390/ma16124333.

[59] P. Šittner, L. Heller, J. Pilch, C. Curfs, T. Alonso, D. Favier, Young's modulus of austenite and martensite phases in superelastic NiTi wires, J. Mater. Eng. Perform. 23 (2014) 2303–2314, https://doi.org/10.1007/s11665-014-0976-x.

[60] A. Zaccaria, F. Migliavacca, G. Pennati, L. Petrini, Modeling of braided stents: comparison of geometry reconstruction and contact strategies, J. Biomech. 107 (2020) 109841, https://doi.org/10.1016/j.jbiomech.2020.109841.

[61] Zwicki Roell, Product Information Materials Testing Machines zwickiLine Z0 . 5 to Z5 . 0 Product Information Materials Testing Machines zwickiLine Z0 . 5 to Z5 . 0, 2022, p. 8.

[62] M.F. Menne, J.W. Schrickel, G. Nickenig, B. Al-Kassou, D. Nelles, T. Schmitz-Rode, U. Steinseifer, O. De Backer, A. Sedaghat, Mechanical properties of currently

available left atrial appendage occlusion devices: a bench-testing analysis, Artif. Organs 43 (2019) 656–665, https://doi.org/10.1111/aor.13414.
[63] InstructionforUseAmuletAmplatzer, (n.d.). https://www.accessdata.fda.gov/cdrh_docs/pdf20/P200049C.pdf (accessed October 24, 2024).
[64] G.M. Bosi, A. Cook, R. Rai, L.J. Menezes, S. Schievano, R. Torii, G. Burriesci, Computational fluid dynamic analysis of the left atrial appendage to predict thrombosis risk, Front. Cardiovasc. Med. 5 (2018), https://doi.org/10.3389/fcvm.2018.00034.
[65] M.T. Lee, V. Martorana, R.I. Md, R. Sivera, A.C. Cook, L. Menezes, G. Burriesci, R. Torii, G.M. Bosi, On preserving anatomical detail in statistical shape analysis for clustering: focus on left atrial appendage morphology, Front. Netw. Physiol. 4 (2024), https://doi.org/10.3389/fnetp.2024.1467180.
[66] C. Capelli, G.M. Bosi, E. Cerri, J. Nordmeyer, T. Odenwald, P. Bonhoeffer, F. Migliavacca, A.M. Taylor, S. Schievano, Patient-specific simulations of transcatheter aortic valve stent implantation, Med. Biol. Eng. Comput. 50 (2012) 183–192, https://doi.org/10.1007/s11517-012-0864-1.
[67] S. Sanatkhani, S. Nedios, P.G. Menon, A. Bollmann, G. Hindricks, S.G. Shroff, Subject-specific calculation of left atrial appendage blood-borne particle residence time distribution in atrial fibrillation, Front. Physiol. 12 (2021) 633135, https://doi.org/10.3389/fphys.2021.633135.
[68] G. Musotto, A. Monteleone, D. Vella, S. Di Leonardo, A. Viola, G. Pitarresi, B. Zuccarello, A. Pantano, A. Cook, G.M. Bosi, G. Burriesci, The role of patient-specific morphological features of the left atrial appendage on the thromboembolic risk under atrial fibrillation, Front. Cardiovasc. Med. 9 (2022), https://doi.org/10.3389/fcvm.2022.894187.
[69] F. Nematzadeh, A computational study of effects of material properties, strain level, and friction coefficient on smart stent behavior and peripheral artery performance during the interaction process, J. Intell. Mater. Syst. Struct. 33 (2022) 703–714, https://doi.org/10.1177/1045389X211026380.
[70] H. Mozafari, P. Dong, S. Zhao, Y. Bi, X. Han, L. Gu, Migration resistance of esophageal stents: the role of stent design, Comput. Biol. Med. 100 (2018) 43–49, https://doi.org/10.1016/j.compbiomed.2018.06.031.
[71] E. Henderson, D.H. Nash, W.M. Dempster, On the experimental testing of fine Nitinol wires for medical devices, J. Mech. Behav. Biomed. Mater. 4 (2011) 261–268, https://doi.org/10.1016/j.jmbbm.2010.10.004.
[72] H.B. Henninger, S.P. Reese, A.E. Anderson, J.A. Weiss, Validation of computational models in biomechanics, Proc. Inst. Mech. Eng. [H] 224 (2010) 801–812.
[73] ASME, VV40-Assessing credibility of computational modeling through verification and validation application to medical devices - asme. https://www.asme.org/codes-standards/find-codes-standards/assessing-credibility-of-computational-modeling-through-verification-and-validation-application-to-medical-devices, 2018. (Accessed 25 November 2024).
[74] FDA, Assessing the credibility of computational modeling and simulation in medical device submissions - guidance for industry and food and drug administration staff. https://www.fda.gov/regulatory-information/search-fda-guidance-documents/assessing-credibility-computational-modeling-and-simulation-medical-device-submissions, 2023.
[75] Romano Setzu, A. Olivares, J. Mill, C. Albors, O. Camara, K. Valen-Sendstad, M. T. Mora, Beatriz Trenor, M. Sermesant, M. Barbier, Building credibility of computational models in cardiovascular medicine through verification and validation 19, EDMA, 2024, pp. 86–90. https://www.europeandissemination.eu/article/building-credibility-of-computational-models-in-cardiovascular-medicine-through-verification-and-validation/21403. (Accessed 24 October 2024).
[76] J. Shirani, J. Alaeddini, Structural remodeling of the left atrial appendage in patients with chronic non-valvular atrial fibrillation: implications for thrombus formation, systemic embolism, and assessment by transesophageal echocardiography, Cardiovasc. Pathol. 9 (2000) 95–101, https://doi.org/10.1016/S1054-8807(00)00030-2.